Inorg. Chem. **2005**, *44*, 2493–2506

d-Electron-Induced Negative Magnetoresistance of a π–d Interaction System Based on a Brominated-TTF Donor

Junichi Nishijo, Akira Miyazaki, and Toshiaki Enoki*

Department of Chemistry, Graduate School of Science and Engineering, Tokyo Institute of Technology, 2-12-1 Ookayama, Meguro-ku, Tokyo 152-8551, Japan

Ryoji Watanabe, Yoshiyuki Kuwatani, and Masahiko Iyoda

Department of Chemistry, Tokyo Metropolitan University, Hachioji, Tokyo 192-0397, Japan

Received October 16, 2004

A new π–d interaction system (EDT-TTFBr$_2$)$_2$FeBr$_4$ (EDT-TTFBr$_2$ = 4,5-dibromo-4′,5′-ethylenedithiotetrathiafulvalene) and its nonmagnetic anion analogue (EDT-TTFBr$_2$)$_2$GaBr$_4$ based on a brominated TTF-type organic donor are investigated. The salts featured by quasi-1D π-electronic systems are metallic with metal–insulator transitions taking place at about 20 and 70 K for the FeBr$_4^-$ and GaBr$_4^-$ salts, respectively, where the low-temperature insulating state is associated with charge ordering or a Mott insulator followed by an antiferromagnetic transition at lower temperatures. The FeBr$_4^-$ salt is featured with an antiferromagnetic transition of the anion d spins at a Néel temperature (T_N) = 11 K, which is significantly high despite its long anion–anion Br–Br contact, suggesting the importance of the π–d interaction in the magnetism. The surprisingly strong π–d interaction, ca. –22.3 K estimated from the magnetization curve, evidences the usefulness of the chemical modification of the donor molecule with bromine substitution to achieve strong intermolecular interaction. The antiferromagnetic state of the anion d spins affects the transport of the conducting π electrons through the strong π–d interaction, as evidenced by the presence of a resistivity anomaly of the FeBr$_4^-$ salt at T_N. Below T_N, the FeBr$_4^-$ salt shows negative magnetoresistance that reaches –23% at the highest magnetic field investigated (B = 15 T), whereas only a small positive magnetoresistance is observed in the π-electron-only GaBr$_4^-$ salt. The mechanism of the negative magnetoresistance is explained by the stabilization of the insulating state of the π electrons by the periodic magnetic potential of the anion d spins in the FeBr$_4^-$ salt, which is modified by applying the external magnetic field.

1. Introduction

In recent years, hybrid "$\pi-$d interaction systems",[1−11] in which conducting π electrons interact with localized magnetic d electrons, have been intensively investigated as a new realm of research in organic-donor-based molecular conductors. They are also attractive for the wide scope of applications for molecule-based electronic devices where the conductivity can be controlled by the magnetic field, for example, large negative magnetoresistance (MR),[6,8] field-induced metal−insulator (MI) transition,[3] and field-induced superconductivity.[5] In these systems, the $\pi-$d interaction can affect conducting π electrons as an internal field, where we can apply not only a spatially uniform but also a spatially oscillating internal field to the π system by using an

* To whom correspondence should be addressed. E-mail: tenoki@chem.titech.ac.jp. Tel: +81-3-5734-2610. Fax: +81-3-5734-2242.

(1) Enoki, T.; Yamaura, J.-I.; Miyazaki, A. *Bull. Chem. Soc. Jpn.* **1997**, *70*, 2005−2023.
(2) Miyazaki, A.; Enomoto, K.; Okabe, K.; Yamazaki, H.; Nishijo, J.; Enoki, T.; Ogura, E.; Ugawa, K.; Kuwatani Y.; Iyoda, M. *J. Solid State Chem.* **2002**, *168*, 547−562.
(3) Kobayashi, H.; Kobayashi, A.; Cassoux, P. *Chem. Soc. Rev.* **2000**, *29*, 325−333.
(4) Sato, A.; Ojima, E.; Akutsu, H.; Nakazawa, Y.; Kobayashi, H.; Tanaka, H.; Kobayashi, A.; Cassoux, P. *Phys. Rev. B: Solid State* **2000**, *61*, 111−114.
(5) Uji, S.; Shinagawa, H.; Terashima, T.; Yakabe, T.; Terai, Y.; Tokumoto, M.; Kobayashi, A.; Tanaka, H.; Kobayashi, H. *Nature* **2001**, *410*, 908−910.
(6) Hanasaki, N.; Tajima, H.; Matsuda, M.; Naito, T.; Inabe, T. *Phys. Rev. B: Solid State* **2000**, *62*, 5839−5842.
(7) Nishijo, J.; Ogura, E.; Yamaura, J.; Miyazaki, A.; Enoki, T.; Takano, T.; Kuwatani, Y.; Iyoda, M. *Solid State Commun.* **2000**, *116*, 661−664.
(8) Enomoto, K.; Miyazaki, A.; Enoki, T. *Bull. Chem. Soc. Jpn.* **2001**, *74*, 459−470.
(9) Coronado, E.; Galán-Mascarós, J. R.; Gomez-García, C. J.; Laukhin, V. *Nature* **2000**, *408*, 447−449.
(10) Ouahab, L.; Enoki, T. *Eur. J. Inorg. Chem.* **2004**, 933−941.
(11) Tokumoto, M.; Naito, T.; Kobayashi, H.; Kobayashi, A.; Laukhin, V. N.; Brossard, L.; Cassoux, P. *Synth. Met.* **1997**, *86*, 2161−2162.

10.1021/ic048548k CCC: $30.25
Published on Web 03/04/2005

antiferromagnetic (AF) d system. Such cooperative features of the electron-transport magnetism of $\pi-$d interaction systems are promising to the future achievement of smaller, highly integrated multifunctional molecule-based devices. However, their $\pi-$d interactions are regrettably not so strong[1−16] in the present stage, in comparison to the s−d interaction in traditional metal-based magnets. This weakness results because the localized magnetic electrons and the conducting electrons are separately placed on different molecules; that is, the former are placed on π-donor molecules and the latter on anion molecules having d electrons. Therefore, to apply the $\pi-$d systems to molecule-based devices, it is indispensable to strengthen the intermolecular interaction. In the meantime, the enhancement of the $\pi-$d interaction is an important issue in molecular conductor physics. Indeed, in the range in which the $\pi-$d interaction is competing with the kinetic energy of the conducting π electrons, a new, basic physics scope will be opened in which it is unknown what may happen given the knowledge on the existing $\pi-$d interaction systems.

In the early stages of research on molecular magnetic conductors, many researchers tried to build appropriate electronic systems with the $\pi-$d interaction enhanced by using molecular design, which can control the properties of the organic donor molecule itself, resulting in various kinds of electronic systems. However, the physical properties are governed not only by the character of the molecule itself but also by the arrangement of the molecules. Unfortunately, it is difficult to control the molecular arrangement at will in molecular conductors because the intermolecular interaction is very weak, and it is well-known that even small changes in the intermolecular interaction and in the conditions of crystal growth cause a change in the molecular arrangement. To solve this problem, there are several suggested works that reveal that an intermolecular attractive interaction can be produced by introducing the orientation-controlling sites in molecules.[17−24] The attractive interaction is weaker than a chemical bond but stronger than an ordinary van der Waals interaction. Though it is still difficult to intentionally control the crystal structure, using donor molecules containing such orientation-controlling sites allows us to control the donor−anion distance.

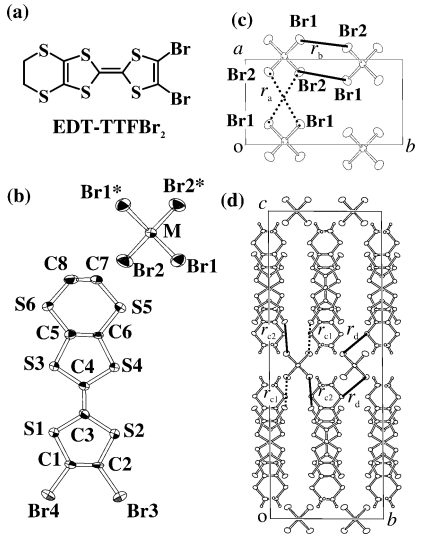

Figure 1. Molecular and crystal structure of $(EDT\text{-}TTFBr_2)_2MBr_4$ (M = Fe, Ga). (a) The structure of the EDT-$TTFBr_2$ donor molecule. (b) A thermal ellipsoid plot (50% probability) of the $FeBr_4^-$ salt drawn by ORTEP-III (ref 33). (c) The arrangement of the anions placed on the $c/2$ plane, projected on the *ab* plane. The dotted lines r_a [= 5.085(8) and 5.130(9) Å for M = Fe and Ga, respectively] and solid lines r_b [= 3.996(8) and 4.007(8) Å for M = Fe and Ga, respectively] represent the anion−anion interchain and intrachain Br1−Br2 contacts, respectively. (d) The crystal structure of $(EDT\text{-}TTFBr_2)_2MBr_4$ projected on the *bc* plane. The dotted lines r_{c1} [= 3.657(8) and 3.685(10) Å for M = Fe and Ga, respectively], solid lines r_{c2} [= 3.673(9) and 3.677(9) Å for M = Fe and Ga, respectively], and solid lines r_d [= 3.683(8) and 3.686(8) Å for M = Fe and Ga, respectively] represent the short donor−anion Br3−Br1, Br4−Br2, and S5−Br1 contacts, respectively.

The bromine-bonded TTF-type donor EDT-$TTFBr_2$ (4,5-dibromo-4′,5′-ethylenedithiotetrathiafulvalene; see Figure 1a) was selected from the donor molecules having orientation-controlling sites and employed in the present work to achieve the strong $\pi-$d interaction. On the same side of the TTF moiety, this donor molecule has two bromine atoms that cause attractive interaction with a halogen atom of a magnetic anion, when halogen-coordinated anions are employed, resulting in the formation of short donor−anion contacts, which are an advantage to achieving a strong $\pi-$d interaction. The other side of TTF moiety is substituted with an ethylenedithio bridge that expands the π orbital and stabilizes the metallic state. Meanwhile, transition-metal complex $FeBr_4^-$ was used as a magnetic anion. The anion has a large magnetic moment $S = {}^5/_2$ and a small size, where the former is suitable for producing a strong $\pi-$d interaction and the latter is preferable for donor molecules to be stacked compactly in forming a high-conductive donor column. Indeed, it is known that several salts of this anion are metallic with strengthened $\pi-$d interactions.[2−3,8,25] In addition, there is a nonmagnetic analogue of the anion, $GaBr_4^-$, where gallium(III) has an ionic radius (0.47 Å) quite similar to that of iron(III) (0.49 Å), which results in the isostructural crystal. The existence of the nonmagnetic analogue is useful in comprehensively investigating the effect of $\pi-$d interaction.

In the present paper, we report the structure and physical properties of $(EDT\text{-}TTFBr_2)_2MBr_4$ (M = Fe, Ga), which are

(12) Sugano, T.; Takenouchi, H.; Shiomi, D.; Kinoshita, M. *Synth. Met.* **1991**, *42*, 2217−2220.
(13) Kepert, C. J.; Kurmoo, M.; Day, P.; Truter, M. R. *Synth. Met.* **1995**, *70*, 781−782.
(14) Day, P.; Kurmoo, M. *Synth. Met.* **1997**, *85*, 1445−1450.
(15) Kurmoo, M.; Day, P.; Guionneau, P.; Bravic, G.; Chasseau, D.; Ducasse, L.; Allan, M. L.; Marsden, I. D.; Friend, R. H. *Inorg. Chem.* **1996**, *35*, 4719−4726.
(16) Mallah, T.; Hollis, C.; Bott, S.; Kurmoo, M.; Day, P. *J. Chem. Soc., Dalton Trans.* **1990**, 859−865.
(17) Schlemper, E. O.; Britton, D. *Acta Crystallogr.* **1965**, *18*, 419−424.
(18) Imakubo, T.; Sawa, H.; Kato, R. *J. Chem. Soc., Chem. Commun.* **1995**, 1097−1098; 1667−1668.
(19) Gompper, R.; Hock, J.; Ploborn, K.; Dormann, E.; Winter, H. *Adv. Mater.* **1995**, *7*, 41−43.
(20) Iyoda, M.; Kuwatani, Y.; Hara, K.; Ogura, E.; Suzuki, H.; Ito, H.; Mori, T. *Chem. Lett.* **1997**, 599−600.
(21) Iyoda, M.; Kuwatani, Y.; Ogura, E.; Hara, K.; Suzuki, H.; Takano, T.; Takeda, K.; Takano, J.-I.; Ugawa, K.; Yoshida, M.; Matsuyama, H.; Nishikawa, H.; Ikemoto, I.; Kato, T.; Yoneyama, N.; Nishijo, J.; Miyazaki, A.; Enoki, T. *Heterocycles* **2001**, *54*, 833−848.
(22) Imakubo, T.; Tajima, N.; Tamura, M.; Kato, R.; Nishio, Y.; Kajita, K.; *J. Mater. Chem.* **2002**, *12*, 159−161.
(23) Suzuki, T.; Fujii, H.; Yamashita, Y.; Kabuto, C.; Tanaka, S.; Tanaka, S.; Harasawa, M.; Mukai, T.; Miyashi, T. *J. Am. Chem. Soc.* **1992**, *114*, 3034−3043.
(24) Domercq, B.; Devic, T.; Fourmigué, M.; Auban-Senzier, P.; Canadell, E. *J. Mater. Chem.* **2001**, *11*, 1570−1575.

investigated on the basis of crystal structure analyses, magnetic susceptibility, electron paramagnetic resonance (EPR), resistivity, and MR, where the negative MR observed in M = Fe is discussed on the basis of the π−d interaction.

2. Experimental Section

EDT-TTFBr$_2$ was prepared according to the procedures available in the literature.[24,26] Black needlelike crystals of (EDT-TTFBr$_2$)$_2$MBr$_4$ (M = Fe, Ga) were obtained by the galvanostatic oxidation (I = 0.25 μA) of EDT-TTFBr$_2$ (8 mg) under an argon atmosphere at 5 °C for 2 weeks, using (n-C$_4$H$_9$)$_4$N[MBr$_4$] (35 mg) and distilled chlorobenzene (15 mL) as the supporting electrolyte and solvent, respectively. Typical crystal sizes were 1 × 0.1 × 0.05 mm^3 for M = Fe and 0.5 × 0.05 × 0.03 mm^3 for M = Ga. The crystal structures for M = Fe and Ga were determined by the single-crystal X-ray diffraction method with a Rigaku AFC-7R four-circle diffractometer at 293 K, using Mo Kα radiation (λ = 0.71 069 Å). The structures were solved using direct methods (SHELXS-86)[27] and then refined with the full-matrix least-squares method (SHELXL-93).[28] An absorption correction based on the Ψ scan was introduced. All non-hydrogen atoms were refined anisotropically, whereas hydrogen atoms were placed in their calculated positions and refined by the riding model. The transfer integrals between donor molecules, the energy band structure, and the magnetic structure of the π−d interaction system were calculated on the basis of the tight-binding approximation, using the extended Hückel parameters.[29] Magnetic susceptibilities were measured by using Quantum-Design MPMS-5 and MPMS-XL superconducting quantum interference device (SQUID) magnetometers for an assembly of aligned single crystals whose typical weight was 0.8−1.2 mg in the temperature range of 2−300 K under a field of up to 7 T. The spin susceptibilities were obtained after the subtraction of the Pascal diamagnetic contribution, χ_{dia} = −5.59 × 10^{-4} and −5.57 × 10^{-4} emu mol^{-1} for the FeBr$_4^-$ and GaBr$_4^-$ salts, respectively, from the observed susceptibilities. The electrical resistivities for both salts were measured using a direct current four-probe technique in the temperature range of 1.5−300 K, where electrodes were cemented by carbon paste onto samples with gold wires (15 μm) and typical crystal sizes were 1 × 0.1 × 0.05 mm^3 and 0.8 × 0.05 × 0.05 mm^3 for M = Fe and Ga, respectively. We used a Be−Cu clamp cell for measuring high-pressure resistivities up to 15 kbar with a pressure medium of Daphne-7243 oil (Idemitsu Kosan Co.). MR was measured using a 15-T superconducting magnet (Oxford Instruments) and a clamp cell at ambient and high pressures. EPR measurements for both salts were carried out with an assembly of aligned single crystals, using an X-band electron spin resonance spectrometer (JEOL JES-TE200) with a continuous-flow He cryostat (Oxford Instruments ESR910) in the temperature range of 4−300 K. Aligned single crystals were mounted on a polytetrafluoroethylene rod and sealed in a sample tube with a thermal exchange gas (He; 20 Torr).

3. Results

3-1. Crystal Structures. The crystal structure of (EDT-TTFBr$_2$)$_2$MBr$_4$ (M = Fe, Ga), which is isostructural regardless of the counteranions, is shown in Figure 1, and the crystallographic data are summarized in Table 1. Though the crystal is classified as $C2/c$ in the standard setting, the space group of $I2/b11$ is suitable to discuss the physical properties, where the crystallographic axes agree with the characteristic axes of the magnetic susceptibility and molecular axes of EDT-TTFBr$_2$. The structure is similar to that of the π−d interaction system (EDO-TTFBr$_2$)$_2$FeBr$_4$ consisting of an oxygen-substituted analogue of the donor[2] except for a difference in the conformation of the ethylenedichalcogen group as follows. In the present crystals, the donors are stacked in a head-to-tail manner to form quasi-one-dimensional (1D) columns elongated parallel to the a axis. The adjacent donor molecules in a donor column of the EDT-TTFBr$_2$ salts are related by a 2_1 axis parallel to the a axis, whereas those of the EDO-TTFBr$_2$ salt are related by the glide symmetry, with a c-glide plane being perpendicular to the long axis of the donor molecular plane. An asymmetric unit contains one crystallographically independent donor molecule and an anion, as shown in Figure 1b. In the arrangement of the anion layer, the interanion Br1−Br2 contacts r_b along the b-axis direction [= 3.996 (8) and 4.007 (8) Å for M = Fe and Ga, respectively] are ca. 3% longer than the sum of the van der Waals radii of the bromine atoms (3.90 Å), whereas interanion Br1−Br2 contacts r_a along the a-axis direction [= 5.085 (8) and 5.130 (9) Å for M= Fe and Ga, respectively] are much longer than the sum of the van der Waals radii. Thus, the anions also form 1D chains elongated parallel to the b axis, which is perpendicular to the donor columns. However, in contrast to an intrachain Br−Br distance of 3.871 (8) Å in (EDO-TTFBr$_2$)$_2$FeBr$_4$, the intrachain Br−Br distance in (EDT-TTFBr$_2$)$_2$MBr$_4$ is significantly longer. Therefore, it is suggested that the direct anion−anion exchange interaction is almost absent between the Fe^{3+} spins in the 1D anion chain.

In contrast to the long anion−anion distances, the attractive interaction between the bromine atoms of the donor and the anion shortens the donor−anion distance; that is, the short atomic contacts r_{c1} of Br3−Br1 [= 3.657 (8) and 3.685 (10)

Table 1. Crystallographic Data

	(EDT-TTFBr$_2$)FeBr$_4$	(EDT-TTFBr$_2$)GaBr$_4$
temperature/K	293(2)	293(2)
formula	C$_{16}$H$_8$Br$_8$Fe$_1$S$_{12}$	C$_{16}$H$_8$Br$_8$Ga$_1$S$_{12}$
fw	1280.11	1293.99
cryst syst	monoclinic	monoclinic
space group	$I2/b11$[a]	$I2/b11$[a]
a/Å	7.066(10)	7.080(12)
b/Å	13.10(2)	13.132(3)
c/Å	35.65(9)	35.627(9)
α/deg	90.26(16)	90.60(2)
β/deg	90	90
γ/deg	90	90
V/Å^3	3300(11)	3312(6)
Z	4	4
reflns collected (2θ < 55°)	3205	3824
reflns unique	2287	2025
R_1 for all data[b]	0.090	0.095
wR_2 for all data	0.132	0.258

[a] In the usual manner, this space group is classified into $C_{2/c}$. [b] $R_1 = \Sigma(||F_0| - |F_C||)/\Sigma|F_0|$. $wR_2 = [\Sigma w(|F_0|^2 - |F_C|^2)^2/\Sigma w(|F_0|^2)^2]^{1/2}$.

(25) Okabe, K.; Enomoto, K.; Miyazaki, A.; Enoki, T. *Mol. Cryst. Liq. Cryst.* **2002**, *376*, 513−518.
(26) Kux, U.; Suzuki, H.; Sasaki, S.; Iyoda, M. *Chem. Lett.* **1995**, 183−184.
(27) Sheldrick, G. M. *SHELXS86*; University of Göttingen: Göttingen, Federal Republic of Germany, 1986.
(28) Sheldrick, G. M. *SHELXL93*; University of Göttingen: Göttingen, Federal Republic of Germany, 1993.
(29) Mori, T.; Kobayashi, A.; Sasaki, Y.; Kobayashi, H.; Saito, G.; Inokuchi, H. *Bull. Chem. Soc. Jpn.* **1984**, *57*, 627−633.

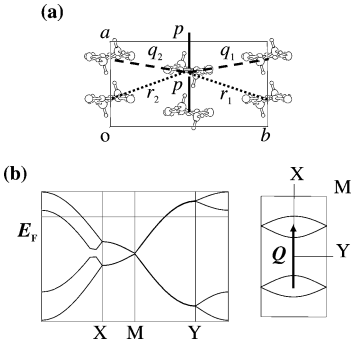

Figure 2. (a) Arrangement of the donor molecules projected on the *ab* plane. Solid, dashed, and dotted lines represent the overlap integrals between the HOMOs of adjacent donor molecules (see text). (b) Band structure (left) and Fermi surface (right) where a solid line E_F and an arrow indicate the Fermi energy and the nesting vector $Q = a^*/2$, respectively.

Å for M = Fe and Ga, respectively] and r_{c2} of Br4−Br2 [= 3.673 (9) and 3.677 (9) Å for M = Fe and Ga, respectively] are ca. 7% shorter than the sum of the van der Waals radii of the bromine atoms. In addition, the attractive intermolecular interaction also causes short S5−Br1 atomic contacts r_d, whose values [3.683 (8) and 3.686 (8) Å for M = Fe and Ga, respectively] are ca. 3% shorter than the sum of the van der Waals radii of the bromine and sulfur atoms (3.80 Å). The long anion−anion distances and the short donor−anion distances enhance the importance of the π−d interaction in the magnetism of the $FeBr_4^-$ salt. It should be noted that each anion molecule has four short Br−Br donor−anion contacts (two r_{c1} and two r_{c2}) and two short S−Br contacts (two r_d) making a bridge between the two donor layers.

The overlap integrals, band structure, and Fermi surface of the donor π-electron system, calculated on the basis of the extended Hückel and tight-binding methods,[29] are shown in Figure 2, where the calculated values of the overlap integrals are $p = -29.8 \times 10^{-3}$, $q_1 = -1.39 \times 10^{-3}$, $q_2 = -1.43 \times 10^{-3}$, $r_1 = 6.71 \times 10^{-3}$, and $r_2 = 6.42 \times 10^{-3}$, and we assume the transfer integral $t = ES$ in calculating the band structure, where S is the overlap integral and the coefficient $E = 10$ eV.[29] As a result of the calculations, the electronic structure of the π electrons is quasi-1D, featuring two lens-shaped Fermi surfaces. From the structure of the Fermi surfaces, it is clear that a nesting vector $Q = a^*/2$ is present, as shown in Figure 2b.

In addition to the donor−donor overlaps, it is expected that the overlap integral between a donor and an anion takes a finite value because of the presence of short donor−anion contacts. For characterizing the electronic features of the donor−anion contacts, information on the wave function distribution of the highest occupied molecular orbit (HOMO) of a donor molecule is particularly important because the interaction is generated by the wave function overlaps between the donor and the anion. For this purpose, the wave function distribution is calculated for an EDT-$TTFBr_2$ molecule on the basis of PM3 method.[30] The HOMO electron is distributed mainly in the TTF moiety and the sulfur atoms of the ethylenedithio group. However, no electron is present in the bromine atoms attached to the TTF skeleton. This fact

(30) Stewart, J. J. P. *J. Comput. Chem.* **1989**, *10*, 209−220.

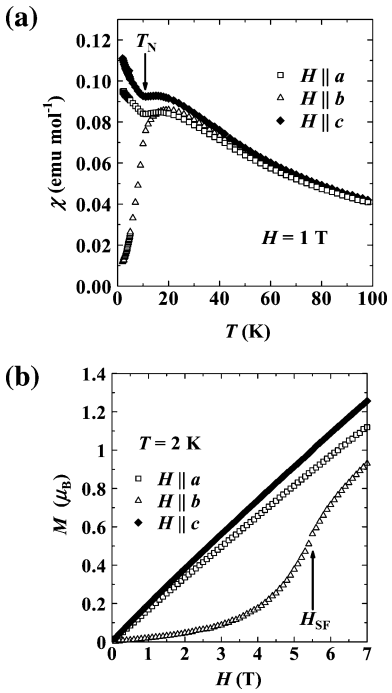

Figure 3. (a) Temperature dependence of the magnetic susceptibilities of (EDT-$TTFBr_2$)$_2$$FeBr_4$ in external field $H = 1$ T applied parallel to the three crystallographic directions. $T_N = 11$ K is the AF transition temperature. (b) The magnetization curves of (EDT-$TTFBr_2$)$_2$$FeBr_4$ at $T = 2$ K in the field applied along the three crystallographic axes. A spin−flop transition takes place at $H_{SF} = 5.8$ T for $H \parallel b$.

indicates that the Br−Br contacts between a donor and an anion do not contribute as importantly to the π−d interaction or the donor−anion electron transfer, whereas the S−Br contact between a donor and an anion can contribute to it. Indeed, the sum of the five overlapping integrals between the HOMOs of a donor molecule and the five between the singly occupied molecular orbitals (SOMOs) of an anion,[31] the latter of which are calculated on the basis of the extended Hückel method consisting of five d orbitals of iron(III) and small contributions of the p orbitals of the bromine ions, has a finite value of 9.3×10^{-4} only at the short donor−anion S5−Br1 contact r_d, whereas the short donor−anion Br−Br contacts, r_{c1} and r_{c2}, give negligible contributions.

3-2. Magnetic Susceptibility of the $FeBr_4^-$ Salt. The magnetic susceptibility χ of the $FeBr_4^-$ salt is shown in Figure 3a, where χ obeys the Curie−Weiss law in the high-temperature region above ca. 150 K, with a Curie constant $C = 4.40$ emu K/mol and an AF Weiss temperature $\Theta = -3.6$ K, the former of which corresponds to one $S = {}^5/_2$ spin of $FeBr_4^-$ per formula unit. Therefore, the magnetism is governed mostly by the Fe^{3+} localized spins, although a minor contribution from the donor π-electron spins is plausible. The susceptibilities have a broad hump of short-range order at around 20 K, and below ca. 11 K, anisotropic behavior emerges between the different field directions. Here, χ increases as the temperature decreases for $H \parallel a$ and c axes, whereas it decreases for $H \parallel b$ axis (H = magnetic field). The appearance of the anisotropic behavior indicates

(31) The calculation method is noted in the following article, and we calculated the donor−anion overlap integral by using their program. Mori, T.; Katsuhara, M. *J. Phys. Soc. Jpn.* **2002**, *71*, 826−844.

the onset of an AF transition at $T_N = 11$ K, where the spin easy axis is oriented parallel to the *b* axis in the ordered state, as evidenced by a decreasing trend of the *b* axis' susceptibility below T_N. The large difference between $|\Theta|$ and T_N ($\Theta < T_N$) indicates that the strength of the AF interaction increases at low temperatures, as will be discussed later. The increase of the *a* and *c* axes' susceptibilities below T_N, accompanied by plateaus at T_N, contradicts the trend in ordinary antiferromagnets. The increase below T_N is also found in λ-$(BETS)_2FeCl_4$ [11] and $(EDO\text{-}TTFBr_2)_2FeBr_4$,[2] though the origin of the increase remains unclear. The T_N value observed in the present salt is quite higher than that expected from the crystal structure, and it should be recollected that the anion−anion distances are considerably longer than the sum of the van der Waals radii. Therefore, such a high T_N suggests that the magnetic moments of the anions are connected by the π−d interaction, which is strong enough to produce such a high transition temperature.

The magnetization curves of the $FeBr_4^-$ salt at 2 K are shown in Figure 3b. The salt has small magnetizations in the whole observed field range up to 7 T, which are only ca. $^1/_5$−$^1/_4$ of the saturated value ($5\,\mu_B$) at the maximum field investigated. Here, the saturation field is roughly estimated as 27 T, which is obtained by extrapolating the linear-fitting line of the *c*-axis magnetization in the low field range ($0 \le H \le 3$ T) to the saturation magnetization value. The magnetizations along the *a* and *c* axes monotonically increase with convex curvatures as the field is raised, whereas the magnetization in $H \parallel b$ axis shows quite smaller values consistent with the spin easy axis being the *b* axis. The magnetization along the *b* axis shows a sudden increase of a spin−flop transition at $H_{SF} \sim 5.8$ T, and the magnetization along the *b* axis is smaller than that of the other two directions, even above H_{SF}. The observed spin−flop field is considerably larger, compared with those of typical $FeBr_4^-$ salts of TTF-type organic donors,[2−3,8,25] as a result of the strong exchange field.

3-3. Electrical Resistivity. The electrical resistivities of the $GaBr_4^-$ salt are measured along the *a* axis, which is parallel to the conducting donor chain, at ambient and high pressures. The pressure dependence of the resistivity at room temperature and the temperature dependence of the resistivity at various pressures are shown in Figures 4a and 5, respectively. The resistivity at room temperature is lowered from 4.2×10^{-2} to 2.4×10^{-2} Ω cm as the pressure is raised from 0 to 11.0 kbar, and no significant difference is observed in the pressure range $11.0 \le P \le 13.4$ kbar. At ambient pressure, the salt has metallic conduction with a resistivity minimum at ca. 120 K. The resistivity slightly increases below this temperature, with no singularity observed, in contrast to that in the $FeBr_4^-$ salt, as will be discussed later. When we apply high pressures, the resistivity and the temperature of a resistivity minimum are reduced. Nevertheless, the increase of the resistivity at low temperatures does not disappear, even at 14.8 kbar. The behavior becomes understandable when we plot the derivative of the resistivity, $\Delta E = \Delta\ln(\rho/\Omega\text{cm})/\Delta(1/T)$, as a function of temperature, as shown in Figure 6. Here, the value ΔE roughly represents

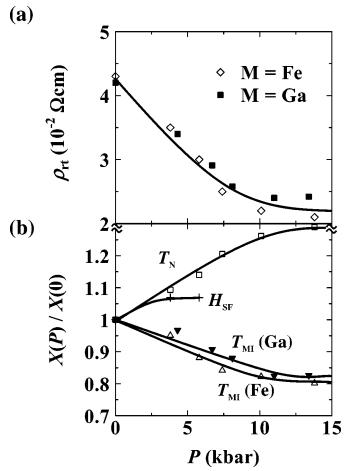

Figure 4. (a) Pressure dependence of the resistivities of the $GaBr_4^-$ and $FeBr_4^-$ salts at room temperature. (b) Pressure dependence of T_N (square), H_{SF} (cross), and T_{MI} (triangle) of the $FeBr_4^-$ salt and T_{MI} (reverse triangle) of the $GaBr_4^-$ salt. The values are normalized by those of ambient pressure. The solid lines are visual guides.

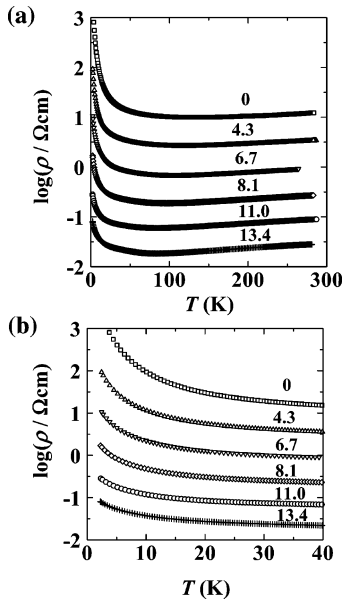

Figure 5. (a) Temperature dependence of the *a*-axis resistivity of $(EDT\text{-}TTFBr_2)_2GaBr_4$ at ambient and high pressures. (b) The enlargement in the low-temperature region. The pressure values are given by the numbers indicated, and the data for 0, 4.3, 6.7, 8.1, and 11.0 kbar are vertically shifted up by 2.5, 2, 1.5, 1, and 0.5, respectively, for clarity in both figures.

the activation energy in the resistivity, where the position of its peak indicates an onset of a MI transition temperature T_{MI}, in the case that an insulating state is stabilized on the low-temperature side of the peak. There are two anomalies in the ΔE versus *T* plot; that is, a peak at higher temperatures, where the temperature of the peak is lowered as the pressure increases, except for T_{MI} at ambient pressure, and a shoulder at lower temperatures $T_s \sim 10$ K, the pressure dependence of which is not so large. The anomaly at higher temperatures is naturally assigned to a MI transition temperature (T_{MI}) from the temperature dependence of the resistivity at low temperatures. It should be noted that the temperature of the peak at ambient pressure (∼48 K) is probably underestimated in the plot because of a technical problem. At low pressures, microcracks may be generated in the sample in a cooling

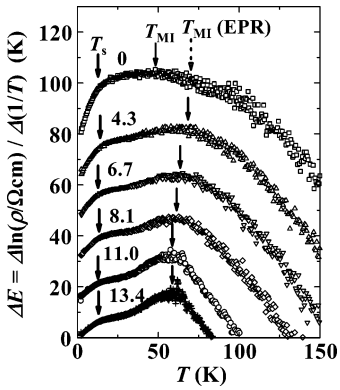

Figure 6. Derivative of the resistivity vs temperature for the $GaBr_4^-$ salt under different pressures. The pressure values are given by the numbers indicated. The data for 0, 4.3, 6.7, 8.1, and 11.0 kbar are vertically shifted up by 75, 60, 45, 30, and 15, respectively, for clarity. The solid arrows indicate the positions of the MI transition temperature (T_{MI}) estimated from the peak of the graph and the shoulders at low temperatures (T_s). The dashed arrow T_{MI} (EPR) indicates the MI transition temperature estimated from the EPR spectra.

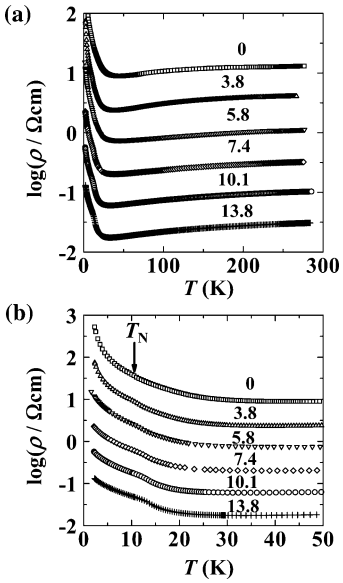

Figure 7. (a) Temperature dependence of the *a*-axis resistivity of (EDT-TTFBr$_2$)$_2$FeBr$_4$ at ambient and high pressures. (b) The enlargement in the low-temperature region. The pressure values are given by the numbers indicated. T_N denotes the Néel temperature. The data for 0, 3.8, 5.8, 7.4, and 10.1 kbar are vertically shifted up by 2.5, 2, 1.5, 1, and 0.5, respectively, for clarity in both figures.

process as a result of thermal contraction, which is in contrast to the high-quality crack-free measurements at high pressures; thus, good quality measurements are impeded at low pressures. Indeed, the EPR results suggest the onset temperature of the MI transition at 70 K, as will be shown later. When we take the MI transition temperature obtained by EPR as the peak position, a pressure-induced linear decrease of T_{MI} is observed in the whole pressure range up to ca. 11 kbar, whereas the resistivity becomes pressure-independent above the pressure, as shown in Figure 4.

The pressure dependence of the resistivities of the $FeBr_4^-$ salt at room temperature and the temperature dependence of the resistivity are shown in Figures 4a and 7, respectively. The resistivity at room temperature is lowered from 4.3×10^{-2} to 2.1×10^{-2} Ω cm as the pressure is raised from 0 to

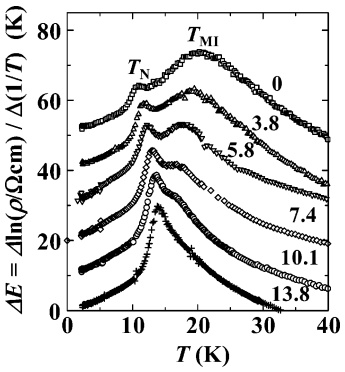

Figure 8. Derivative of the resistivity vs temperature for the $FeBr_4^-$ salt at ambient and high pressures. The pressure values are given by the numbers indicated. The data for 0, 3.8, 5.8, 7.4, and 10.1 kbar are vertically shifted up by 50, 40, 30, 20, and 10 K, respectively, for clarity. T_{MI} and T_N represent the MI transition temperature and the Néel temperature, respectively.

13.8 kbar. In contrast to the $GaBr_4^-$ salt, the $FeBr_4^-$ salt takes a resistivity minimum at ca. 40 K at ambient pressure. To clarify the resistivity anomalies, the derivative of the resistivity is plotted as shown in Figure 8. At ambient pressure, ΔE has a broad hump at ca. 20 K, below which the resistivity clearly increases, indicating an onset of a MI transition at this temperature. Figure 4b presents the pressure dependence of T_{MI}. It is lowered upon the elevation of pressure in a manner similar to that of the $GaBr_4^-$ salt. Below the MI transition temperature, an additional hump of ΔE is observed at $T_N = 11$ K, where the localized d spins of $FeBr_4^-$ exhibit an AF transition. The fact that the magnetic ordering of the d electrons affects the transport properties of the π electrons clearly indicates the important role of the $\pi-$d interaction, which is caused by the short donor−anion contacts. As shown in Figure 8, the temperature of the anomaly at T_N increases as the pressure is raised; in contrast to that, T_{MI} decreases as the pressure increases. Then, these two anomalies of T_{MI} and T_N merge above 13.8 kbar. The pressure dependence of T_N is shown in Figure 4b.

3-4. Magnetoresistances. To investigate the effect of the $\pi-$d interaction at different pressures, MR was measured at various pressures, where the current *I* and the magnetic field *H* were applied parallel to the *a* axis (donor stacking axis) and the *b* axis (easy axis of $FeBr_4^-$ anions), respectively. Parts a and b of Figure 9 present the field dependence of the MRs of the $GaBr_4^-$ and $FeBr_4^-$ salts at $T = 1.5$ K, respectively.

The $GaBr_4^-$ salt shows only small, positive MRs in the whole field range investigated, where the MR increases quadratically, regardless of the pressure in the low field region up to ca. 3 T. In the high field region, the slope of the MR versus *H* plot is gradually reduced, giving an *S*-shaped field dependence, and finally, the MR tends to become saturated. The reduction of the slope and the saturated behavior are weakened by applying pressure, where the MR becomes more linear-field-dependent in the high field region. In any case, the MR value of the nonmagnetic $GaBr_4^-$ salt is in the range of ca. 2.5−3.5% below that at 15 T.

In contrast, the $FeBr_4^-$ salt shows large, pressure-dependent, negative MRs. The MR of the $FeBr_4^-$ salt is steeply lowered with a convex curvature followed by the appearance

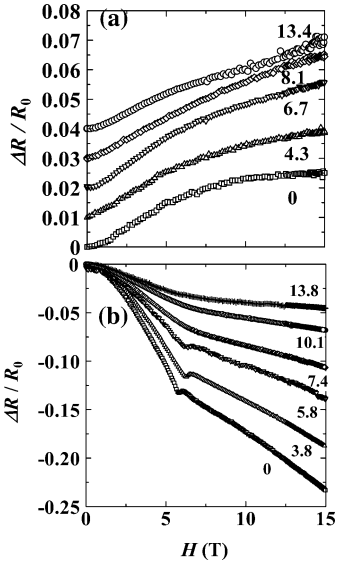

Figure 9. MRs of the (a) $GaBr_4^-$ and (b) $FeBr_4^-$ salts at different pressures at 1.5 K. The data of 4.3, 6.7, 8.1, and 13.4 kbar of the $GaBr_4^-$ salt are shifted up by 0.01, 0.02, 0.03, and 0.04, respectively, for clarity. The current I and external magnetic field H are applied parallel to the a and b axes, respectively. The pressure values are given by the numbers indicated.

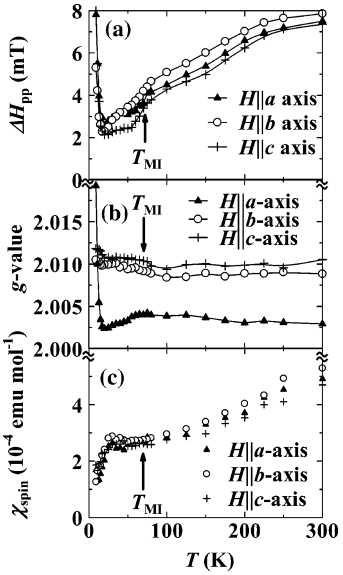

Figure 10. Temperature dependence of (a) the EPR line width, (b) the g values, and (c) the EPR spin susceptibility along the three crystallographic axes for $(EDT\text{-}TTFBr_2)_2GaBr_4$. T_{MI} denotes the MI transition temperature. The absolute values of the susceptibility are obtained by comparing the EPR intensity with the static susceptibility from the SQUID measurement at room temperature.

of a kink, at which the spin−flop transition takes place, in the low pressure range up to 7.4 kbar. The large, negative MR and the anomaly at the spin−flop transition are convincing evidences of the existence of the π−d interaction. Above the spin−flop transition, the slope of the MR versus field curve becomes moderate and the MR reaches −23% at $H =$ 15 T at ambient pressure. Judging from the pressure-induced increase of the field of the kink, the spin−flop transition field is elevated from 5.8 to 6.2 T as the pressure goes from 0 to 3.8 kbar and takes a constant value in the pressure range $3.8 \leq P \leq 5.8$ kbar, as shown in Figure 4b. Above 7.4 kbar, the kink disappears, although a trace of the kink is evidenced as a slope change in the field at which it occurs. The disappearance of the kink suggests the ineffectiveness of the d-electron spins in the π-electron transport in the high-pressure range, where the metallic features are enhanced. This is supported by the reduction of the negative MR as the pressure increases. The value of MR at $H = 15$ T and the highest pressure $P = 13.8$ kbar is only 19% of that at ambient pressure.

3-5. EPR. The $GaBr_4^-$ salt shows a Lorentzian-shaped EPR signal with peak-to-peak line widths $\Delta H = 7.50$, 7.86, and 7.35 mT and g values $g = 2.003$, 2.009, and 2.011 for $H \parallel a$, b, and c axes, respectively, at room temperature. The anisotropy in the g value is in good agreement with the orientation of the donor molecule; that is, the lowest g value corresponds to the field direction applied perpendicular to the molecular plane, whereas the g value becomes the highest in the field applied along the long side of the molecular plane.[32]

As shown in Figure 10a, the values of ΔH hold the relation $\Delta H_b > \Delta H_a > \Delta H_c$ down to ca. 30 K. The line widths gradually decrease with a convex curvature as the temperature is lowered down to 70 K, at which they show an abrupt drop. Different samples of the different batches show the anomaly at the same temperature, suggesting that the anomaly is not a result of the low quality of the crystal but, rather, indicates the genuine phase transition of the π electrons. Judging from the fact that the temperature dependence of the resistivity shows no anomaly at that temperature except for an increase of the resistivity below it, the transition at 70 K is concluded to be the MI transition. Indeed, such a drop of ΔH is frequently observed in EPR measurements attributed to the MI transition.[33] In the insulating phase of the π electrons below $T_{MI} = 70$ K, the EPR signal can be observed down to ca. 10 K. The existence of paramagnetic π spins observable by EPR below T_{MI} indicates that the insulating ground state is neither the charge density wave nor the spin density wave state. In the temperature range $20 \leq T < T_{MI}$, ΔH shows a complicated behavior; that is, ΔH along the three axes has a plateau around 40 K, followed by a decrease below ca. 30K, where ΔH_b becomes smaller than ΔH_a. Judging from the decrease of the spin susceptibility below 30 K, as will be mentioned below, the decrease of ΔH below 30 K can be related to an AF short-range order, although the details remain unclear. Finally, ΔH starts increasing divergently below 20 K, with the EPR signal disappearing at ca. 10 K. The divergent behavior of ΔH is suggestive of a precursor of a long-range AF ordering of the π electrons,[34,35] followed by an AF long-range ordering taking place at 10 K. The agreement between this temperature and T_s, the temperature of the anomaly in the resistivity of the $GaBr_4^-$ salt, indicates that the anomaly at T_s is assigned to an AF transition of the π electrons.

(32) Sugano, T.; Saito, G.; Kinoshita, M. *Phys. Rev. B: Solid State* **1986**, *34*, 117−125.
(33) Nakamura, T. *J. Phys. Soc. Jpn.* **2003**, *72*, 213-216.
(34) Mori, H. *Prog. Theor. Phys.* **1963**, *30*, 578−580.
(35) Tazuke, Y.; Nagata, K. *J. Phys. Soc. Jpn.* **1975**, *38*, 1003−1010.

The angular dependence of ΔH also changes at T_{MI}. Above T_{MI}, the angular dependence of ΔH is well-explained on the basis of the conventional angular-dependent behavior for the system that the spin−lattice relaxation governs

$$\Delta H(\theta) = \Delta H_a \cos^2\theta + \Delta H_c \sin^2\theta \quad (1)$$

where ΔH_a and ΔH_c, are the EPR line widths along the *a* and *c* axes, respectively, and θ is the direction between the applied field and *a* axis. Contrary to the behavior observed above T_{MI}, ΔH shows more complicated behavior; for example, ΔH along the *ac* plane at 45 K increases from 3.11 to 3.28 mT as the angle measured from the *a* axis is changed from 0° to 30°, and then ΔH decreases and takes a minimum value of 2.39 mT at $H \parallel c$ axis.

The effects of the MI transition, the short-range ordering below 20 K, and the AF transition are also clearly seen in the change in the *g* values, as shown in Figure 10b. The *g* values are roughly temperature-independent above T_{MI}. Below T_{MI}, the *g* values along the *b* and *c* axes gradually increase, whereas that of the *a* axis gradually decreases. The *g* value increases suddenly below 20 K, along the *a* axis, which is, again, suggestive of the development of magnetic short-range ordering, followed by the long-range ordering at 10 K, where the *g* value diverges.

The spin susceptibility χ_{spin}, which is estimated from the intensity of the EPR spectra and calibrated by using the susceptibility measured by SQUID at room temperature ($= 5.0 \times 10^{-4}$ emu·mol^{-1}), is shown in Figure 10c. The observed value of χ_{spin} at room temperature is in the typical range of the Pauli paramagnetism of organic conductors.[36] χ_{spin} gradually decreases as the temperature decreases down to ca. 70 K. Below that temperature, χ_{spin} takes a constant value of ca. 2.7×10^{-4} emu mol^{-1}, followed by a steep decrease below 30 K, and the EPR signal disappears at ca. 10 K. The static susceptibility behaves in a manner similar to that of the EPR susceptibility in the temperature range above ca. 20 K. The steep drop of χ_{spin} is considered to be associated with a precursor of the AF transition.

In the case of $(EDT\text{-}TTFBr_2)_2FeBr_4$, despite the coexistence of the π and d electrons, only one broad signal is observed in the EPR spectra in the temperature range investigated because of the coalescence of the signals of the two kinds of electrons, suggesting the presence of the interaction between these two spins. The values of the line width ΔH at room temperature are 86, 129, and 56 mT for $H \parallel a$, *b*, and *c* axes, respectively. The values are in the same range as that of the well-separated $FeBr_4^-$ anion in CH_3CN solution (55 mT).[37] In addition, the angular dependence of ΔH obeys eq 1 in the whole temperature range where the angular dependence is observed ($T > 30$ K). This angular dependence is different from the dipolar line width of the anions calculated from the crystal structure, which has a minimum at the magic angle (54.7°) in both *ac* and *bc* planes, where the angle is measured from the *a* and *b* axis, respectively. These facts suggest that the spin−lattice relaxation of the $FeBr_4^-$ anion, not the spin−spin relaxation, is dominant in the line widths at temperatures above ca. 30 K. The small contribution of the dipolar line width is probably due to the exchange narrowing caused by exchange interactions between the π and d electrons. ΔH has a rather simple temperature dependence, as shown in Figure 11a, compared to that of the $GaBr_4^-$ salt. ΔH_b and ΔH_c gradually increase as the temperature decreases, whereas that of the *a* axis is roughly constant down to ca. 40 K. Below ca. 30 K, ΔH increases in all of the field directions as the temperature is lowered, which is related to the development of the short-range ordering of the $FeBr_4$ anions, followed by the divergence of ΔH at $T_N = 11$ K.

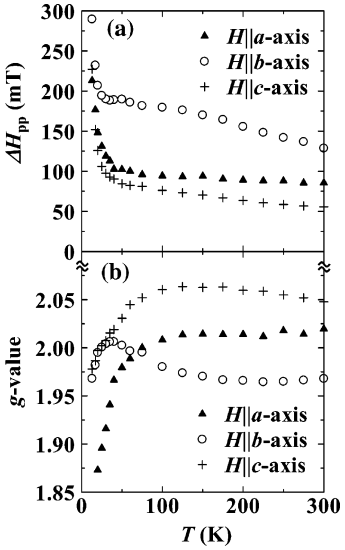

Figure 11. Temperature dependence of (a) the EPR line width and (b) the *g* value of the $FeBr_4^-$ salt measured along the three crystallographic axes.

In contrast, the *g* values show curious behavior at low temperatures. The *g* values take values of $g = 2.02$, 1.97, and 2.05 for $H \parallel a$, *b*, and *c* axes, respectively, at room temperature. The values along the *a* and *b* axes are roughly independent of the temperature down to ca. 150 K, as shown in Figure 11b, whereas that along the *c* axis gradually increases as the temperature decreases. Below 150 K, the *g* values along the *a* and *c* axes slightly decrease, which is followed by a steep decrease below 30 K that is due to the AF short-range ordering. In contrast to these two axes, the *g* value along the *b* axis gradually increases, with a maximum value at ca. 35 K, and then it decreases. The increase of the *g* value along the *b* axis is accompanied by a change in the trend of the angular dependence of the *g* value. Indeed, the angular dependence of the *g* value shows anomalous behavior, especially in $H \parallel bc$ plane, as shown in Figure 12. In usual cases, the angular dependence of the *g* value can be described as

$$g(\theta) = g_b \cos^2\theta + g_c \sin^2\theta \quad (2)$$

where g_b and g_c are the *g* values along the *b* and *c* axes, respectively. At room temperature, the angular dependence

(36) For example, Kagoshima, S.; Nagasawa, H.; Sambongi, T. *One-Dimensional Conductors*; Springer-Verlag: New York, 1989; pp 64−71.
(37) Rodriguez, F.; Moreno, M. *Transition Met. Chem.* **1985**, *10*, 351.

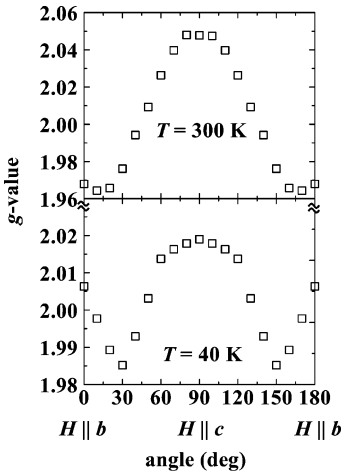

Figure 12. Angular dependence of the *g* value, with *H* || *bc* plane, of the $FeBr_4^-$ salt at 300 and 40 K.

of the *g* value in *H* || *bc* plane is approximately represented by eq 2, except for the presence of a small anomaly observed near $\theta \sim 0°$ and 180°, where a minimum of the *g* value exists at around 10° and 170°. The anomaly becomes larger and more clear at 40 K, where the angular dependence of the *g* value is far from the behavior described by eq 2. The observed anomalous angular dependence is also observed in *H* || *ac* plane, although the anomaly is not as large in this plane. It may be possible to explain the origin of the anomaly as a small misalignment of crystals in the *ac* plane. However, the large discrepancy between eq 2 and the observed value in the *bc* plane at $T = 40$ K cannot be explained only by that. In other words, the angular dependence of the *g* value cannot be explained by a conventional *g*-tensor scheme; the origin of the anomalous angular dependence of the *g* value remains unclear.

4. Discussion

4-1. The Ground State of $(EDT\text{-}TTFBr_2)_2MBr_4$. This discussion is first devoted to the ground state of the π electrons in $(EDT\text{-}TTFBr_2)_2GaBr_4$. For clarifying the ground state, the features of the EPR signal are indispensable. The experimental finding that an EPR signal survives even below T_{MI}, with the line width being divergent at ca. 10 K, indicates that the $GaBr_4^-$ salt is paramagnetic ($10 < T < T_{MI} \sim 70$ K) and AF ($T < 10$ K) in the two low-temperature insulating states, where the π electrons behave as localized magnetic electrons. These multiple transitions can be tracked by the temperature-dependent behavior of the *g* values below T_{MI} shown in Figure 10b. In general, the temperature-dependent changes in the *g* values in the three crystallographic axes below T_{MI} are explained in terms of the changes in the orientations of the donor molecules. In this case, the rotation of the molecules with any rotational axis brings the *g* values close to each other because three crystallographic axes agree with the principal axes of the donor molecule. However, this is not the case in the present experimental findings. Therefore, the change in the *g* values just below T_{MI} is probably caused by the change in the electronic state of the π electrons, though the details remain unclear. The divergence of the *g* value along the *a* axis and the roughly constant values of those along the *b* and *c* axes around 10 K are understood to be the effect of the AF short-range order. According to investigations of typical 1D AF magnets,[38] the *g* value along the chain direction gradually increases, whereas that perpendicular to the chain decreases under the effect of spin fluctuation. This is just the case with the $GaBr_4^-$ salt, where the donor chain is aligned parallel to the *a* axis and the rapid increase of the *g* value is observed in this direction, whereas the decrease of the *g* values along the other directions are obscure as a result of the small misalignment of the crystals and the rapid increase of the *g* value along the *a* axis. There are two typical candidates for the magnetic insulating state: a Mott insulator and a charge ordering state. Though it is difficult to decide which state is stabilized, it should be noted that there is a $\mathbf{S}_\pi = {}^1/_2$ spin per two donors due to the ${}^3/_4$-filled state in any case, where the adjacent two donors form a pair along the 1D chain direction parallel to the *a* axis; that is, there is either a donor dimer in the Mott insulator scenario or a neutral−cationic ($S = 0$ and ${}^1/_2$, respectively) pair in the charge ordering state scenario.

Next, we move on to the $FeBr_4^-$ salt. Though the electronic states below T_{MI} are roughly the same in both salts, as evidenced by the similar temperature dependencies of the resistivities, a large difference between them is present in the MI transition temperatures; that is, $T_{MI} = 20$ and 70 K for the $FeBr_4^-$ and $GaBr_4^-$ salts, respectively. Because these two salts have the same crystal structure, as a result of the quite similar ionic radii of Fe^{3+} and Ga^{3+}, the difference in T_{MI} is considered to originate from the difference in the electronic structures of the anions. It is natural to assume that the electronic structures of the π electrons are the same between the two salts when we consider the same strengths of the on-site Coulomb interaction *U*, inter-site Coulomb interaction *V*, and transfer integrals *t*. However, the transfer integral $t_{\pi d} = 9.3 \times 10^{-3}$ eV between a donor and an anion in the $FeBr_4^-$ salt can affect the electronic structure differently than that in the $GaBr_4^-$ salt. The most important feature of the $FeBr_4^-$ anion is the open shell structure of the iron(III) atom, $(e)^2(t_2)^3$, whereas the $GaBr_4^-$ anion has the closed shell structure, $(e)^4(t_2)^6$; that is, an electron can be transferred from a donor layer to the adjacent donor layer through the open shell of the $FeBr_4^-$ anion by $t_{\pi d}$, for which the two short donor−anion S5−Br1 contacts r_d are responsible for $t_{\pi d}$, as shown in Figure 1d. The interlayer transfer integral $t_{\pi d}$ between the donor and the anion is significantly larger than that between the donor molecules (∼0), resulting in an enhancement of the 3D character of the π electrons such as that in Cu-DCNQI-type salts.[39] Eventually, because of the MI transition inherited by the low dimensional instability, T_{MI} is lowered down to 20 K as a result of the contribution of a fraction of 3D character.

The weakly enhanced 3D character of the $FeBr_4^-$ salt mentioned above does not change the fundamental basis of

(38) Nagata, K.; Tazuke, Y. *J. Phys. Soc. Jpn.* **1972**, *32*, 337−345.
(39) Uji, S.; Terashima, T.; Aoki, H.; Brooks, J. S.; Kato, R.; Sawa, H.; Aonuma, S.; Tamura, M.; Kinoshita, M. *Phys. Rev. B: Solid State* **1994**, *50*, 15597−15601.

the insulating AF ground state from that of the $GaBr_4^-$ salt because of the smallness of $t_{\pi d}$, which is only $^1/_{30}$ and $^1/_6$ of the intra- and interchain transfer integrals between donors, respectively. The same ground state for both salts is also suggested from the similarity of the AF transition temperatures of the π electron of the $GaBr_4^-$ salt and that of the d spins of the $FeBr_4^-$ salt. As will be discussed later, the AF interaction between the π and d spins is much larger than the thermal energy at T_N of the $FeBr_4^-$ anions. Thus, it is suggested that T_N depends crucially on the AF ordering of the π spins because the d spins are strongly coupled to the π spins by a strong $\pi-$d interaction, whereas the direct d$-$d interaction is negligibly weak as a result of the long anion$-$anion distance. Consequently, T_N of the π spins in the $FeBr_4^-$ salt is regarded as the same as that of the d spins, $T_N = 11$ K, which is in good agreement with T_s of the π spins in the $GaBr_4^-$ salt ($\sim$10 K).

Finally, we discuss the pressure dependence of the MI transition. T_{MI} of both salts monotonically decreases by ca. 20% upon an increase in pressure, up to ca. 10 kbar, and then it becomes pressure-independent. The pressure-induced change in T_{MI} behaves similarly to the pressure dependence of the resistivity at room temperature shown in Figure 4a, which is governed by the change in the interdonor transfer integrals induced by lattice contraction. In the crystals of (EDT-TTFBr$_2$)$_2$MBr$_4$, it is expected that the application of pressure makes the intermolecular distances largely shortened along the stacking direction (= the *a* axis), whereas the pressure-induced contraction along the other directions is small, as generally observed in TTF-type donor-based organic conductors.[40] Therefore, the pressure dependence of T_{MI} is ascribed to the increase of the intrachain transfer integral, which decreases the energy gap and lowers the MI transition temperature.

4-2. The Magnetic Structure of the $FeBr_4^-$ Salt and the Strengths of the $\pi-\pi$ and $\pi-$d Interactions. To clarify the magnetic structure of the $FeBr_4^-$ salt, it is important to discuss the effect of the $\pi-$d interaction on electron transport. In (EDT-TTFBr$_2$)$_2$FeBr$_4$, the magnetic structure of the d spins is associated with that of the π spins because only the $\pi-$d interaction couples the d spins, taking into account that the d$-$d interaction is negligibly small. As discussed in the previous section, the ground state of the π electrons at low temperatures is featured with an AF ordered state, where two donors possess a localized spin of $S = ^1/_2$. In general, the AF $\pi-\pi$ interaction J_{ij} between donors i and j is roughly in proportion to $-t_{ij}^2/U$, where t_{ij} is the transfer integral between the donors. Therefore, the large intrachain ($-$298 meV) and small interchain transfer integrals ($-$14 to $+$67 meV) suggest that the π electrons form a 1D Heisenberg AF structure. Then, the d spins having $\mathbf{S}_d = ^5/_2$ participate in the magnetism through the $\pi-$d interaction. An $FeBr_4^-$ anion has six short donor$-$anion contacts: four Br$-$Br contacts and two S$-$Br contacts, as shown in Figure 1, where only the S$-$Br contacts r_d work as the paths of the $\pi-$d interaction because the overlap integrals of the Br$-$Br contacts are negligibly small. Consequently, each $FeBr_4^-$ anion has two $\pi-$d interaction paths to two donor pairs belonging to adjacent donor planes above and beneath the anion, whereas each donor pair on a donor plane has two $\pi-$d interaction paths to adjacent $FeBr_4^-$ anions. The magnetic structure expected from the 1D AF π spin structure and the $\pi-$d interaction paths is shown in Figure 13, where the d spins are considered to be coupled in an antiparallel arrangement with the nearest neighbor π spins through the strong $\pi-$d interaction $J_{\pi d}$, and the 1D AF chains of the π spins on a donor layer are weakly coupled with each other by the interchain interactions $J_{2\pi\pi}$.

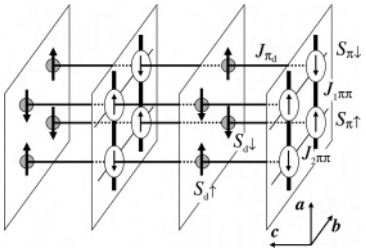

Figure 13. Schematic four-sublattice magnetic structure of (EDT-TTFBr$_2$)$_2$FeBr$_4$ consisting of two π-spin sublattices ($S_{\pi\uparrow}$ and $S_{\pi\downarrow}$) and two d spin sublattices ($S_{d\uparrow}$ and $S_{d\downarrow}$). Gray circles, white ellipses, and the thick and thin arrows indicate the anion, donor pair, and the d and π spins, respectively. Each d spin is connected to two donor pairs by $J_{\pi d}$ (solid line along the *c* direction), whereas the π spins of the donor pairs are antiferromagnetically connected through strong intrachain $J_{1\pi\pi}$ (thick solid line along the *a* direction) and weak interchain $J_{2\pi\pi}$ (dotted line along *b* direction) interactions.

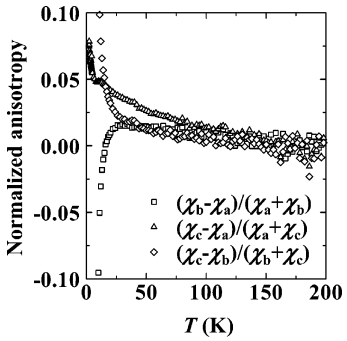

Figure 14. Normalized anisotropies of the magnetic susceptibilities of (EDT-TTFBr$_2$)$_2$FeBr$_4$ with $H = 1$ T.

Here, we summarize the experimental findings on the correlation between the donor π electrons and the anion d-electron spins. In the high-temperature region above T_{MI}, the metallic π electrons have small spin densities at the donor sites. Therefore, the AF interaction between the π and d electrons is weak, as evidenced by the small absolute value of $\Theta = -3.6$ K estimated in the high-temperature region well-above T_{MI}. When the temperature is lowered to near $T_{MI} = 20$ K, the π electrons start behaving as localized spins, which strongly interact antiferromagnetically with the anion d spins. The effect of the localized spins of the π electrons is clearly seen from the anisotropy in the susceptibility, as shown in Figure 14. The anisotropies have small values in the high-temperature region $T > 25$ K. Below 25 K, the anisotropies $(\chi_c - \chi_b)/(\chi_c + \chi_b)$ steeply increase as the temperature is lowered, whereas the anisotropies $(\chi_b - \chi_a)/(\chi_b + \chi_a)$ rapidly decrease and become negative. Considering

(40) For example, Enoki, T.; Tsujikawa, K.; Suzuki, K.; Uchida, A.; Ohashi, Y.; Yamakado, H.; Yakushi K.; Saito, G. *Phys. Rev. B: Solid State* **1994**, *50*, 16287$-$16294.

the fact that the temperature 25 K is in the vicinity of T_{MI}, the generation of the localized spins upon the MI transition is considered to trigger the change in the anisotropies, strengthening the $\pi-$d interaction. Below T_{MI}, the d spins are affected by the fluctuations of the π spins, which are coupled with each other through the strong $\pi-\pi$ interaction and interacting with the d spins through the strong $\pi-$d interaction. According to the EPR results of the $GaBr_4^-$ salt, the AF transition of the π spins takes place at ca. 10 K, whereas the d spins undergo an AF transition at 11 K for the $FeBr_4^-$ salt. The coincidence of the AF transition temperatures between the π and d spins clearly demonstrates the important role of the $\pi-$d interaction that bridges between both spin systems.

Next, we estimate the strengths of the $\pi-\pi$ and $\pi-$d interactions on the basis of the experimental results and the magnetic structure model employed in Figure 13. First, the strength of the $\pi-\pi$ interaction is estimated from the susceptibility of the $GaBr_4^-$ salt exhibited in Figure 10c. The observed susceptibility of the $GaBr_4^-$ salt shows weak temperature dependence in the temperature range $25 < T < 70$ K, which is the natural consequence of the 1D Heisenberg AF system with a strong intrachain AF interaction $J_{1\pi\pi}$. Indeed, the absolute value and general temperature independence of the susceptibility are well-fitted to the Bonner−Fisher model[41,42] with magnetic moment $\mathbf{S}_\pi = {}^1/_2$ per donor pair and $J_{1\pi\pi} = -290$ K. It is not surprising that the value $J_{1\pi\pi} = -290$ K is smaller than that expected from the relation $-t^2/U = -1030$ K, where we suggest $U = 1$ eV. Strictly speaking, t in the relation $J = -t^2/U$ is not a transfer integral between adjacent donors but that between sites having $S = {}^1/_2$ spins; that is, t is the transfer integral between donor dimers in the Mott insulator or donor pairs in the charge ordering state. In the Mott insulating state, the wave function of a localized π electron spreads over a dimer, resulting in a smaller coefficient of the wave function at an atom compared with that that spreads over a donor molecule. In addition, dimerization increases and decreases the intra- and interdimer transfer integrals, respectively. On the other hand, localized π electrons in the charge ordering state are located on every other donor molecule in a donor chain, resulting in the longer spin−spin distance and smaller J value. It is noted that, despite the quantitative discrepancy of transfer integral t mentioned above, we can roughly estimate the dimensionality of π spins in a qualitative level by using the value of t between adjacent donors because of the following two reasons. First, dimerization or charge ordering reduces not only the intrachain but also the interchain transfer integrals. Therefore, the change in the ratio of intra- to interchain transfer integrals is not so large. Second, the intrachain transfer integral is exceedingly larger than that of the interchain. Therefore, the small change in the transfer integrals is not critical in discussing the dimensionality. Then,

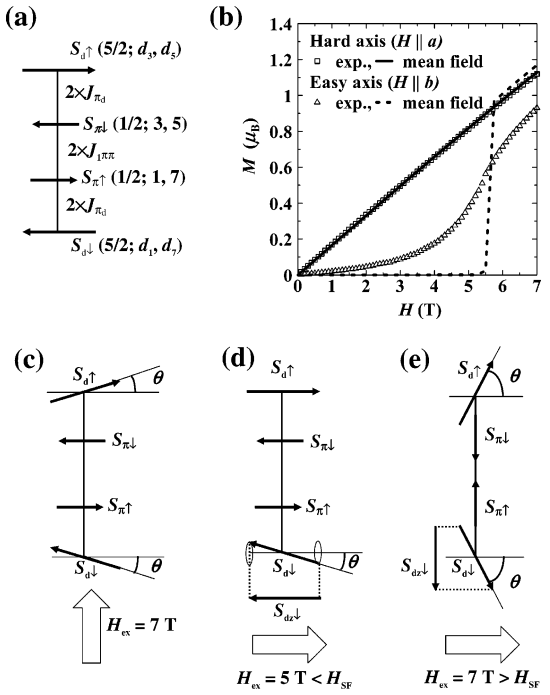

Figure 15. (a) Schematic model of the magnetic structure of the $FeBr_4^-$ salt, where the weak interchain interaction $J_{2\pi\pi}$ of the donor pairs is neglected. $\mathbf{S}_\pi$ and $\mathbf{S}_d$ represent the $S = {}^1/_2$ π spin at a donor pair and the $S = {}^5/_2$ d spin at an anion, respectively. $S_{\pi\uparrow}$ ($S_{\pi\downarrow}$) interacts with two $S_{\pi\downarrow}$ ($S_{\pi\uparrow}$) and two $S_{d\downarrow}$ ($S_{d\uparrow}$) through $J_{1\pi\pi}$ and $J_{\pi d}$, respectively. (b) Mean-field fittings of the magnetizations along the a and b axes, with values of $J_{\pi d} = -22.3$ K and anisotropy energy $K_u = 0.9$ K for both π and d spins, accompanied by the experimental results. The experimental results and the mean-field fittings are carried out at $T = 2$ K. (c) The calculated spin structure of the $FeBr_4^-$ salt in $H_{ex} = 7$ T is applied parallel to the hard axis, and that in (d) $H_{ex} = 5$ T ($< H_{SF}$) and (e) $H_{ex} = 7$ T ($> H_{SF}$) are applied parallel to the easy axis. Spin angle θ is estimated to be 13.4° for both $S_{d\uparrow}$ and $S_{d\downarrow}$ in part c, ~0° and 0.01° for $S_{d\uparrow}$ and $S_{d\downarrow}$, respectively in part d, and 166.1° for both $S_{d\uparrow}$ and $S_{d\downarrow}$ in part e. $S_{dz\uparrow}$ and $S_{dz\downarrow}$ indicate the components of $S_{d\uparrow}$ and $S_{d\downarrow}$ parallel to $\mathbf{S}_\pi$.

the strength of the $\pi-$d interaction is estimated on the basis of the value of $J_{1\pi\pi}$ and the mean-field calculation. The magnetic structures of donors and anions are approximately represented by four sublattices consisting of two π spin sublattices ($S_{\pi\uparrow}$, $S_{\pi\downarrow}$) and two d spin sublattices ($S_{d\uparrow}$, $S_{d\downarrow}$), which have up ($S_{\pi\uparrow}$, $S_{d\uparrow}$) and down ($S_{\pi\downarrow}$, $S_{d\downarrow}$) components, as shown in Figure 13. Interchain $\pi-\pi$ interaction $J_{2\pi\pi}$ is neglected in the donor layer because of the quasi-1D character of the π-electron system. Therefore, each π spin interacts with two π and two d spins through $J_{1\pi\pi}$ and $J_{\pi d}$, respectively; for example, $S_{\pi\uparrow}$ interacts with two $S_{\pi\downarrow}$'s along the chain parallel to the a axis and with two $S_{d\downarrow}$'s placed beneath and above the donor layer. This feature of the interactions is schematically displayed in Figure 15a. On the basis of this four-sublattices model and the mean-field approximation (see the Appendix), the observed magnetizations along the a axis (hard axis) and b axis (easy axis) at 2 K are theoretically reproduced with $J_{\pi d}$ and magnetic anisotropy K_u as adjustable parameters. In the calculation, the same anisotropy energy is assumed for both the π and d spins for simplicity. As shown in Figure 15b, the calculated magnetizations with values of $J_{\pi d} = -22.3$ K and $K_u = 0.9$ K are in good agreement with the observed magnetizations, reproducing the presence of the spin−flop transition and the convex curvature

(41) Bonner, J. C.; Fisher, M. E. *Phys. Rev. A: At., Mol., Opt. Phys.* **1964**, *135*, A640−A658.
(42) Brown, D. B.; Donner, J. A.; Hall, J. W.; Wilson, S. R.; Wilson, R. B.; Hodgson, D. J.; Hatfield, W. E. *Inorg. Chem.* **1979**, *18*, 2635−2639.

of the magnetization along the easy and hard axes, respectively. The value of $J_{\pi d}$ is much stronger than that of ordinary $\pi-d$ systems[1−16] as a result of the short donor−anion S−Br contacts, which are achieved by the strong attractive interaction between the bromine atoms of brominated TTF and $FeBr_4^-$.

The details of the magnetic structure of the $FeBr_4^-$ salt calculated on the basis of the mean-field approximation are shown in parts c, d, and e of Figure 15 for three actual cases with a field applied along different axes. When we apply the field H_{ex} along the hard axis, both d spins $S_{d\uparrow}$ and $S_{d\downarrow}$ are canted by the field, whereas the π spins almost maintain the antiparallel arrangement as a result of their strong AF interaction $J_{1\pi\pi}$, as shown in Figure 15c. In contrast, only $S_{d\downarrow}$ is canted when the field $H_{ex} < H_{SF}$ is applied parallel to the easy axis, whereas $S_{d\uparrow}$ is stabilized by the Zeeman energy (Figure 15d) and the π spins tend to be in an antiparallel arrangement. When the field becomes larger than the spin−flop field H_{SF}, both π and d spins are rotated as shown in Figure 15e, where both d spins $S_{d\uparrow}$ and $S_{d\downarrow}$ are canted and the π spins take an antiparallel arrangement similar to the case where H_{ex} is applied along the hard axis. Here, it should be noted that the obtained magnetic structure could well explain the convex curvature of the magnetization curves observed along the hard axis (see Figures 3b and 15b). The linear field dependence of the magnetization along the hard axis of the ordinary antiferromagnet is ascribed to the field-induced rotations of the spins in all of the magnetic sublattices. In contrast to the ordinary antiferromagnets, the d spins interact only with the π spins in the $FeBr_4^-$ salt, where the π spins are in an approximately antiparallel arrangement because of the strong intrachain AF interaction. In this condition with H_{ex} along the hard axis, the internal field $H_{\pi d}$ of the π spin to the d spin is approximately perpendicular to the external field, as shown in Figure 15c, as a result of the small canting angles of the π spins. From the geometries of the spins and the internal field, magnetization M is approximately described only by the magnetization of the d spins, which reproduce the observed convex curvature, whereas the π spins do not contribute to the magnetization because of their antiparallel configuration.

Finally, we briefly comment on the pressure effect on the magnetism. The spin−flop transition field H_{SF} increases only from 5.8 to 6.2 T as the pressure is raised from 0 to 3.8 kbar, and it seems to be independent of pressure above 3.8 kbar. When the relation $H_{SF} = (H_E H_A)^{1/2}$, where H_E and H_A are the exchange field and the anisotropy field, respectively, and the pressure-insensitive nature of the anisotropy, irrespective of its origin between the single-ion and dipolar anisotropies, are taken into account, the pressure dependence of H_{SF} represents the pressure-induced change in the strength of the $\pi-d$ interaction $J_{\pi d}$. Therefore, the observed pressure dependence of H_{SF} suggests the less pressure-sensitive nature of the $\pi-d$ interaction. Here, we have a structural feature specific to the present salts, which is related to the strong, attractive donor−anion interaction along the c axis, in which the $\pi-d$ interaction paths are formed. The c axis is already reduced by the strong, attractive interaction, even at the ambient pressure, which brings about the less pressure-sensitive nature of the $\pi-d$ interaction. In contrast to the pressure insensitivity of $J_{\pi d}$, T_N is more sensitive to the applied pressure. T_N, which is governed by the AF transition of the π electrons, depends on the two-dimensionality of the π spins; that is, T_N largely depends on the interchain AF interactions of the π spins. Because the pressure-induced change in the interchain interaction along the c axis is small, as discussed above, the increase of T_N is attributed to the increase of the interchain interaction $J_{2\pi\pi}$ along the b axis.

The competition between the MI and AF transitions in the $FeBr_4^-$ salt should also be addressed as an consequence of the pressure effect. In the insulating state, because of the localized electronic state of the π electrons, the superexchange interaction is featured with a short-range interaction. Therefore, the pressure-induced change in the structure sensitively affects the AF transition, which is obviously understood from the steep increase in T_N. Under pressures higher than 13.8 kbar, T_N and T_{MI} tend to merge, as shown in Figure 8, suggesting that the AF transition is subjected to the metallic electronic feature of the π electrons under higher pressures. In the metallic phase, the long-range π-conduction−electron-mediated interaction between the d electron spins, which is an analogue of the Ruderman−Kittel−Kasuya−Yoshida interaction in traditional metal magnets, plays a major role. Moreover, the insensitive feature of the MR in the vicinity of the MI transition around 14 kbar is considered to be associated with the magnetism in the conducting medium.

4-3. The Effect of the π-d Interaction on Electron Transport and the Origin of the Negative MR in the $FeBr_4^-$ Salt. On the basis of the magnetic structure obtained above, we discuss the effect of the $\pi-d$ interaction on the electron transport of the π-electron system, in which the negative MR is observed. Below T_N, the AF ordered state of the $FeBr_4^-$ d spins generates a periodic magnetic potential on the π-electron system in the low-temperature magnetic insulating state. Namely, the periodic potential of the d spins induced by the spin polarization of the π electrons counteraffects the π-electron system in a manner similar to the case of the spin density wave state, where the periodic potential of spin-polarized π electrons affects the π electron itself.[43] In the present salt, the periodicity of the potential of the d spins is, certainly, the same as that of the π-electron system, as shown in Figure 13, resulting in the stabilization of the spin-polarized state of the π electrons. Consequently, the localized d spins of the $FeBr_4^-$ anions can enhance the gap of the insulating π-electron system. In the meantime, when a high magnetic field is applied to the system, the periodic potential is weakened as a result of the destabilization of the AF structure of the d spins, where the enhancement of the gap is reduced, resulting in the observed negative MR.[2, 8, 25]

To confirm this idea, we calculated the MR of the $FeBr_4^-$ salt on the basis of the strength of the periodic magnetic

(43) For example, Grüner, G. *Density Waves in Solids*; Addison-Wesley Longmans Inc.: Reading, MA, 1990.

potential of d spins, which is estimated from the magnetization and magnetic structures shown in parts d and e of Figure. Here, we consider the case of H || easy axis for a comparison with the experimental results. When the fact that the component of d spin $\mathbf{S}_d$ parallel to π spin $\mathbf{S}_\pi$ can produce the periodic potential to the π electrons is taken into account, the energy of the $\pi-$d interaction is described as $-2J_{\pi d}\mathbf{S}_\pi\mathbf{S}_d = -2J_{\pi d}|\mathbf{S}_\pi|S_{dz}$, where S_{dz} is the component of $\mathbf{S}_d$ parallel to $\mathbf{S}_\pi$ (see Figure 15d,e). Therefore, it is necessary to determine the value of S_{dz} for calculating the enhanced gap of the insulating π electrons. In the following discussion, to estimate S_{dz}, the collinear AF structure of the π-electron spins is assumed, which is justified by the result of the mean-field calculation where the π electrons almost hold the antiparallel arrangement as a result of the strong intrachain AF interaction $J_{1\pi\pi}$, as shown in parts d and e of Figure 15. According to the result shown in Figure 15d, in the region of $H_{ex} < H_{SF}$, magnetization M, consisting of the spins from the four sublattices, is given by the following equations with $S_{dz\uparrow}$ and $S_{dz\downarrow}$, where the π spins have no contribution as a result of their antiparallel arrangement:

$$M = \frac{1}{2}g(|S_{d\uparrow}| - |S_{d\downarrow}|\cos\theta)$$

$$= \frac{1}{2}g\left(\frac{5}{2} - \frac{5}{2}\cos\theta\right) \quad (4)$$

$$S_{dz\uparrow} = \frac{5}{2} \quad (5)$$

$$S_{dz\downarrow} = -\frac{5}{2}\cos\theta$$

$$= -\frac{5}{2} + \frac{2M}{g} \quad (\therefore \text{eq } 4) \quad (6)$$

where factor $^1/_2$ on the right side of eq 4 means that a formula unit contains half of the two anion sublattices $S_{d\uparrow}$ and $S_{d\downarrow}$. Using eqs 5 and 6, and assuming $g = 2$ for the g value of $FeBr_4^-$ anions, we can estimate S_{dz} from the magnetization M. Similar to $H_{ex} < H_{SF}$, S_{dz} in the field region $H_{ex} > H_{SF}$ can be estimated from the following equations based on the magnetic structure shown in Figure 15e;

$$M = \frac{1}{2}g(|S_{d\uparrow}| + |S_{d\downarrow}|)\cos\theta$$

$$= \frac{5}{2}g\cos\theta \quad (7)$$

$$S_{dz\uparrow} = \frac{5}{2}\sin\theta = \frac{5}{2}\sin\left[\cos^{-1}\left(\frac{2M}{5g}\right)\right] \quad (8)$$

$$S_{dz\downarrow} = -\frac{5}{2}\sin\theta = -\frac{5}{2}\sin\left[\cos^{-1}\left(\frac{2M}{5g}\right)\right] \quad (9)$$

Because the magnetization measurement was carried out only in the field region $H_{ex} < 7$ T because of experimental limitations, we assume a linear field dependence of M in the field range from H_{SF} to 15 T, the maximum field investigated in the MR measurements, to estimate the value of S_{dz} on the basis of eqs 8 and 9. The magnetic potential caused by $S_{d\uparrow}$ and $S_{d\downarrow}$ can be decomposed into the spatial oscillating component in the a direction (V_{osc}) and the uniform component (V_{uni}), as expressed in eqs 10 and 11:

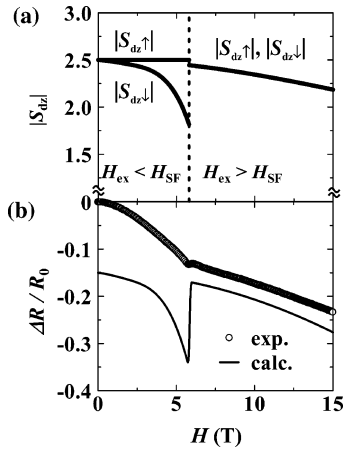

Figure 16. (a) z component of the d spins calculated from the fitting of the observed magnetization curve and eqs 5, 6, 8, and 9 (see text). (b) Field dependence of the observed and calculated MRs with the proportional constant $\alpha = 0.11$ meV. The calculated value is vertically shifted down by 0.15 for clarity.

$$V_{osc} = |2J_{\pi d}|\frac{S_{dz\uparrow} - S_{dz\downarrow}}{2} \quad (10)$$

where only the oscillating component enhances the energy

$$V_{uni} = |2J_{\pi d}|\frac{S_{dz\uparrow} + S_{dz\downarrow}}{2} \quad (11)$$

gap of the AF insulating state of the π electrons and the gap enhancement ΔE_g is in proportion to $|V_{osc}|$. To compare the actual case with the model mentioned above, the MR is calculated on the basis of the estimated values of S_{dz}. The resistivity ρ in the insulating state having an enhancement of the band gap ΔE_g is described as

$$\rho = \rho_0 \exp\left(\frac{\Delta E_g}{k_B T}\right)$$

$$= \rho_0 \exp\left[\frac{1}{k_B T}\frac{\alpha(S_{dz\uparrow} - S_{dz\downarrow})}{2}\right] \quad (12)$$

where ρ_0 is the resistance when the gap enhancement caused by the d spins is absent and α is the proportional constant consisting of $J_{\pi d}$ and the response function of the π-electron system. Using eqs 5, 6, 8, 9, and 12, MR is calculated with $\alpha = 0.11$ meV:

$$\frac{\Delta\rho}{\rho_0} = \frac{\rho(H_{ex}) - \rho(0)}{\rho(0)} \quad (13)$$

and it is shown in Figure 16b. The resistivity gradually decreases with a convex curvature as the field is raised and is followed by a discontinuous jump at H_{SF} that is the result of the jump of S_{dz} at H_{SF}, as shown in Figure 16a. Above H_{SF}, the resistivity gradually decreases again. The field dependence of MR is in semiquantitatively good agreement with that of the observations, proving that the origin of the

negative MR is the effect of the strong $\pi-$d interaction, which causes the periodic potential on the π-electron system.

5. Conclusion

Isostructural salts (EDT-TTFBr$_2$)$_2$MBr$_4$ (M = Fe, Ga) form a donor−anion sandwiched layer structure, where the donor layer consists of 1D metallic donor chains elongated parallel to the *a* axis and the anions form chains parallel to the *b* axis with a large intrachain interval on the anion layer. In these salts, significantly short donor−anion contacts are produced as a result of the strong attractive coordination-bond-like interaction between the bromine atoms of the anion and the donor molecules. The short contacts contribute to the strong donor−anion electronic interaction, whereas the longer interanion Br−Br contact is responsible for a weak interanion interaction on the anion layer.

In the electronic structure, the short donor−anion contacts work as the path of the interlayer electron transfer in the $FeBr_4^-$ salt, which has the open shell Fe^{3+} state, resulting in the stabilization of the metallic state down to 20 K, whereas the closed shell anion analogue, the $GaBr_4^-$ salt, causes a MI transition at 70 K. In addition, the short donor−anion contacts, which enhance the strength of the $\pi-$d interaction, play an essential role in the magnetism of the $FeBr_4^-$ salt. The $FeBr_4^-$ salt takes an AF transition at $T_N = 11$ K, which is much larger than one would expect from the long anion−anion distance, accompanied by the anomaly of the resistivity at this temperature. These findings demonstrate the importance of the $\pi-$d interaction. The strength of the $\pi-$d interaction is estimated as -22.3 K from the magnetization curve, which is the largest ever found among the TTF-based magnetic conductors.

Below T_N, the periodic potential of the d spins, which is caused by the AF arrangement of the π-electron spins, affects the insulating π electrons, where the periodic potential of the d spins stabilizes the magnetic insulating state of the π electrons through the strong $\pi-$d interaction. The stabilization of the insulating state of the π electrons is clearly shown in both the temperature dependence of the resistivity and the MR of the $FeBr_4^-$ salt. As expected from the stabilization effect of the periodic potential of d spins, the resistivity shows an additional increase at T_N, and a large negative MR is observed below that temperature. The negative MR is the natural consequence of the gap enhancement by the d spins. When the high field is applied, the periodic potential is weakened by the Zeeman energy of the d spins, resulting in a reduction of the enhanced gap. Molecular field treatment with the experimental results can explain the negative MR semiquantitatively, in which the role of the $\pi-$d interaction is crucial.

In conclusion, we emphasize the importance and effectiveness of the orientation-controlling sites to achieve the strong $\pi-$d interaction. Introducing functional groups such as halogen atoms makes it easy to shorten donor−anion distances, resulting in the generation of a strong interaction between conducting π and magnetic d electrons, and (EDT-TTFBr$_2$)$_2$FeBr$_4$ provides us an important example.

Acknowledgment. This work was supported by Grants-in-Aid for Scientific Research (Grants 12046231 and 15073211) and a Grant-in-Aid for the 21st Century COE Program "Creation of Molecular Diversity and Development of Functionalities" from the Ministry of Education, Culture, Sports, Science and Technology, Japan. J.N. was supported by a Grant-in-Aid for JSPS Fellows.

Supporting Information Available: Crystallographic data for (EDT-TTFBr$_2$)$_2$MBr$_4$ (M = Fe, Ga) in CIF format. This material is available free of charge via the Internet at http://pubs.acs.org.

Appendix

Mean-Field Calculation of the Magnetization of the $FeBr_4^-$ Salt. When the value of the intrachain $\pi-\pi$ interaction $J_{1\pi\pi}$ and the magnetic structure shown in Figure 15a are used, the strength of the $\pi-$d interaction $J_{\pi d}$ can be estimated. In the calculation, we assume that the spins can be rotated only in a plane including the easy axis, and both π and d spins have the same in-plane anisotropy energy and g values, $g = 2$, for simplicity. The mean field H_m and effective magnetic moment M_m of magnetic sublattice m (= $\pi\uparrow$, $\pi\downarrow$, d$\uparrow$, and d$\downarrow$) are represented as follows:

$$H_{\pi\uparrow} = \frac{2J_{1\pi\pi}}{N_A g^2 \mu_B{}^2} M_{\pi\downarrow} + \frac{2J_{\pi d}}{N_A g^2 \mu_B{}^2} M_{d\downarrow} + H_{anis}$$

$$H_{\pi\downarrow} = \frac{2J_{1\pi\pi}}{N_A g^2 \mu_B{}^2} M_{\pi\uparrow} + \frac{2J_{\pi d}}{N_A g^2 \mu_B{}^2} M_{d\uparrow} + H_{anis}$$

$$H_{d\uparrow} = \frac{2J_{\pi d}}{N_A g^2 \mu_B{}^2} M_{\pi\downarrow} + H_{anis}$$

$$H_{d\downarrow} = \frac{2J_{\pi d}}{N_A g^2 \mu_B{}^2} M_{\pi\uparrow} + H_{anis} \quad \text{(A1)}$$

where $B_S(x)$, S_m, and H_{anis} are the Brillouin function, the spin

$$M_m = N_A g \mu_B S_m \frac{H_m}{|H_m|} B_S\left(\frac{S_m g \mu_B |H_m|}{k_B T}\right) \quad \text{(A2)}$$

of sublattice m ($\mathbf{S}_\pi = {}^1/_2$ and $\mathbf{S}_d = {}^5/_2$), and the anisotropy field, respectively. The calculation is carried out until M_m, the initial value of which is randomly selected, becomes self-consistently determined. If the calculated values of M_m depend on the set of initial values because of the existence of the local minima, we select the state, which has the lowest energy E defined as follows after several trials:

$$E = -4J_{\pi d}(M_{\pi\uparrow}M_{d\downarrow} + M_{\pi\downarrow}M_{d\uparrow}) - 4J_{1\pi\pi}M_{\pi\uparrow}M_{\pi\downarrow} + \sum_m g\mu_B H_{ex} M_m + \sum_m K_u \sin^2\theta m \quad \text{(A3)}$$

where K_u and θ_m are the coefficient of the anisotropy, which is assumed as uniaxial for simplicity, and the angle between the easy axis and the magnetization of sublattice m, respectively. Then, the magnetization M is defined as $M = |\sum_m M_m|$.

IC048548K